Report on a problem studied at the Virtual Physiological Human Network of Excellence Study Group Nottingham 2009
< https://mmsg.mathmos.net/vph-noe/2009/doming-epithelial-cells/ >

# Modelling doming in epithelial monolayers

*Problem presented by:* Paul Appleton
*Report prepared by:* John Fozard, Gareth Jones, Anna Lovrics, Martin Nelson
*Other participants in the study group:* Oliver Jensen, John King, Ida Pu

30th October 2009

## 1 Introduction

In tissue development and rearrangement — and in connection with diseases — very little is known about mechanical parameters that allow certain types of behaviour. In order to experimentally measure in a controlled environment some of these parameters, *in vitro* experiments are performed. Mathematical modelling of these experiments can help identify the most important or sensitive parameters, make parameter estimates of experimentally non-measurable quantities and suggest new experiments.

When grown on rigid substrates in confluent monolayers, MDCK (Madin–Darby canine kidney) cells and other epithelial cell lines form 'dome' structures. Cells start proliferating in appropriate culture conditions and when a confluent monolayer of cells is achieved then cells can lift up from the solid support yet remain continuous with the monolayer, forming characteristic domes. These domes grow, then collapse, and usually re-form in the same place.

Altogether, very little is known about the doming process. It was discovered in 1969 [9, 2] through experiments on epithelial cell lines and it soon became apparent that fluid build-up beneath the cells was the driving factor in dome formation, presumably due to ion transport. When grown on flexible, semi-permeable filters, domes are not formed, and it seems well established that $Na^+/K^+$-ATPase activity is crucial for dome formation. Signalling pathways are also likely to play a role in this process. Certain cellular properties such as adhesion between cells, adhesion between cells and the substrate, the permeability of the cellular junctions and cellular stretchiness change the dynamics of dome formation.

### 1.1 Life cycle of an epithelial dome

In order to successfully model the mechanics of an epithelial dome, we need to understand the mechanisms underlying its growth and subsequent collapse. The key steps are illustrated in Figure 1.

The process begins once the cultured cells reach confluence, forming a coherent single layer of cells. MDCK and other dome-forming cell lines are notable for their characteristic water-pumping property — as a by-product of transporting ions across the cell layer. Consequently a volume of water forms between the cells and the substrate. This causes the bonds that attach the cells to the substrate to be stretched. Eventually, a critical water volume is reached, at which the bonds are broken at a small region of the tissue. This is the incident that marks a dome's formation. This blistering of the tissue causes water to be drawn from nearby regions of the tissue, thus relieving the tension in the attachment bonds at those regions.

However, the cells continue pumping water, and the domes will continue to grow as bonds at the edge of the dome are severed. Concurrently, the tension in the dome increases. At a certain critical tissue tension, the cell layer loses its coherence, and some (perhaps all) of the water escapes from the blister. The cell layer then re-forms at a lower tension, and the process begins again — although the bonds will have no time to reform, explaining why domes (almost) always reform at the same position as a previous dome.

### 1.2 Report summary

In this report we will summarise the progress made in the study group towards developing a mechanical model of dome formation. Such models are not readily found in the literature; among these is a model of Tanner

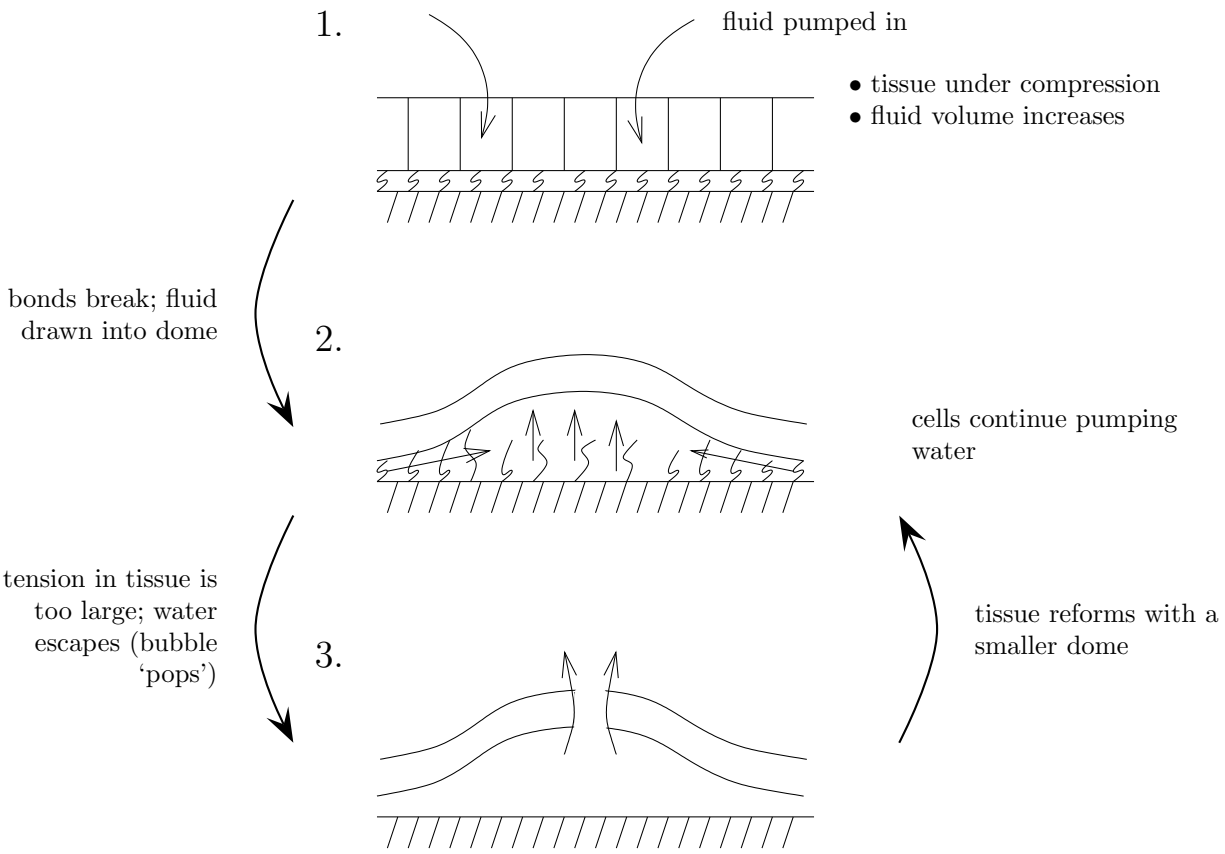


Figure 1: A diagram of the hypothesised mechanism behind dome formation and development.

*et al.* [15], who assume the domes to be hemispherical and use experimental measurements of the doming process to infer the stiffness of the epithelial cell layer.

In the study group we only considered the dome formation process in a one-dimensional beam, approximating the two-dimensional tissue encountered in experiments. In Section 2 we will derive the one-dimensional (1D) model from the full two-dimensional model (which is in turn derived in Appendix A). Following an estimation of the parameters in the 1D model, it will be analysed numerically in Section 3. Conclusions and further avenues for research are detailed in Section 4.

# 2 Modelling

We will model the doming process by assuming that the epithelial cell layer itself is a solid plate, and that the bonding between the cell layer and the substrate is a porous adhesive layer. For a full derivation of the system and for the scalings of the dimensional quantities please see Appendix A.

The full (dimensionless) system of equations are shown below, and comprise 11 equations to be solved for the following 11 dependent variables:

- $w$ — normal displacement of the plate,
- $u_1$, $u_2$ — tangential displacement of the plate,
- $p_1$, $p_2$, $p_3$ — tractions applied to the plate (tangential, tangential, normal),

- $\chi$ — the Airy stress function in the plate,
- $p^{\text{fluid}}$ — the hydrostatic pressure in the fluid,
- $P_{11}$, $P_{12}$, $P_{22}$ — particular solutions to equation (2) below.

The equations are as follows:

$$\frac{1}{2}(u_{\alpha,\beta}+u_{\beta,\alpha})+\left(\frac{\Delta_n^2}{\Delta_t L}\right)\frac{1}{2}w_{,\alpha}w_{,\beta}=\left(\frac{L\Gamma}{\Delta_t}\right)\gamma^{\text{g}}_{\alpha\beta}+\left(\frac{L^2p^*}{D\Delta_t}\right)E_{\alpha\beta\lambda\mu}P_{\lambda\mu}+\varepsilon_{\lambda\gamma}\varepsilon_{\mu\delta}E_{\alpha\beta\lambda\mu}\chi_{,\gamma\delta}, \tag{1}$$

$$P_{\alpha\beta,\beta}+p_\alpha=0 \qquad \text{(particular solution)}, \tag{2}$$

$$\left(\frac{B\Delta_n}{p^*L^4}\right)\nabla^4 w-\varepsilon P_{\alpha\beta}w_{,\alpha\beta}-2\left(\frac{D\Delta_n\Delta_t}{p^*L^3}\right)[w,\chi]-p_3=0, \tag{3}$$

$$\left(\frac{\Delta_t}{L\Gamma(1-\nu^2)}\right)\nabla^4\chi+\left(\frac{\Delta_n^2}{\Gamma L^2}\right)[w,w]=\varepsilon_{\alpha\beta}\varepsilon_{\lambda\mu}\left(\gamma^{\text{g}}_{\alpha\mu,\beta\lambda}+\left(\frac{Lp^*}{D\Gamma}\right)E_{\alpha\mu\gamma\delta}P_{\gamma\delta,\beta\lambda}\right), \tag{4}$$

$$p_\alpha=-\frac{2\Delta_n}{\Delta_t}\left(1+w-\frac{W_0}{\Delta_n}\right)\exp\left(1-u_1^2-u_2^2-\left(w-\frac{W_0}{\Delta_n}\right)\right)u_\alpha, \tag{5}$$

$$p_3=-\left(w-\frac{W_0}{\Delta_n}\right)\exp\left(1-u_1^2-u_2^2-\left(w-\frac{W_0}{\Delta_n}\right)\right)+\left(\frac{\mu\mathscr{Q}L^2}{\Delta_n^3p^*}\right)p^{\text{fluid}}, \tag{6}$$

$$\frac{\partial w}{\partial t}=Q-\boldsymbol{\nabla}\cdot\left(\frac{\kappa}{\alpha^2}\boldsymbol{\nabla}p^{\text{fluid}}\right), \tag{7}$$

where

$$\kappa=\frac{2}{\alpha}\tanh\frac{\alpha w}{2}-w, \tag{8}$$

$$\alpha=\frac{6\sqrt{5}W_{\min}}{d}\frac{1}{w}\left(1-\frac{W_{\min}}{\Delta_n w}\right)^{-3/2}. \tag{9}$$

A subscript preceded by a comma indicates partial differentiation with respect to that coordinate (*e.g.* $\gamma_{12,12}=\partial^2\gamma_{12}/\partial x_1\partial x_2$). Greek subscripts range over $(1,2)$ and the summation convention applies (repeated suffices in a term are summed over $1,2$). We also note the notation $[A,B]=\frac{1}{2}(A_{,11}B_{,22}-2A_{,12}B_{,12}+A_{,22}B_{,11})$. The Levi-Civita tensor $\varepsilon_{\alpha\beta}$ and the fourth-order tensor $E_{\alpha\beta\lambda\mu}$ are both defined in Appendix A.

As input to the model we have the two independent variables $Q$, representing the (dimensionless) rate of fluid flow through the tissue per unit area ('pumping rate'), and $\gamma^{\text{g}}_{\alpha\beta}$, which is the (scaled) growth tensor, indicating how much the tissue has grown (thereby introducing a stress field into the tissue). We also have a large number of parameters, whose values should ideally be gleaned from experimental investigations. These are listed in Table 1.

## 2.1 Model simplification

During the study group a much simpler model was studied. The most significant simplification was the restriction to a one-dimensional beam rather than a plate. Thus we let $u_2=0$, $p_2=0$, $\gamma^{\text{g}}_{12}=\gamma^{\text{g}}_{21}=\gamma^{\text{g}}_{22}=0$, and $u_1$ and $w$ are both independent of $x_2=y$. Furthermore we assume that the tangential traction is zero, *i.e.* $p_1=0$ (giving $P_{\alpha\beta}=0$), and that the growth term $\gamma^{\text{g}}_{11}$ and pumping rate $Q$ are both constant (and hence equal to unity). We eventually find from (1) and (4) that the Airy stress function is given (without loss of generality) by

$$\chi=\frac{T}{2}(\nu x^2+y^2), \tag{10}$$

where $T$ is some constant. Writing $u_1=u$, equation (1) gives us

$$\frac{\partial u}{\partial x}+\left(\frac{\Delta_n^2}{\Delta_t L}\right)\frac{1}{2}\left(\frac{\partial w}{\partial x}\right)^2=\left(\frac{L\Gamma}{\Delta_t}\right)+T \tag{11}$$

| Quantity | Description |
|---|---|
| $p^*$ | Maximum normal traction in debonding |
| $\Delta_n$ | Separation at which max. normal traction achieved |
| $\Delta_t$ | Separation at which max. tangential traction achieved |
| $W_0$ | Separation at which traction is zero |
| $W_{\min}$ | Separation at which layer is of zero porosity |
| $d$ | Distance between bonds |
| $\mu$ | Fluid viscosity |
| $\mathscr{Q}$ | Scale of pumping rate |
| $B$ | Layer bending stiffness |
| $D$ | Layer stretching stiffness |
| $\nu$ | Layer Poisson ratio |
| $\Gamma$ | Scaling of layer growth strain |
| $L$ | Characteristic length of disturbances |

Table 1: Table of physical parameters forming part of the doming model, classified according to their origin: bond-related, fluid dynamics, epithelial mechanics, and phenomenological.

which can be integrated over the domain $(x_L, x_R)$ of the beam, with a zero-displacement condition at the ends, to give

$$T = \left(\frac{\Delta_n^2}{\Delta_t L}\right) \frac{1}{2(x_R - x_L)} \int_{x_L}^{x_R} \left(\frac{\partial w}{\partial x}\right)^2 \mathrm{d}x - \left(\frac{L\Gamma}{\Delta_t}\right). \tag{12}$$

This allows us to solve the system without explicitly considering the tangential displacement $u$. Since $\chi_{,22} = T$, equation (12) is substituted into (3). Eventually, following a rescaling of $T$, we obtain the following system to be solved for the normal displacement $w$:

$$\left(\frac{B\Delta_n}{p^* L^4}\right) \frac{\partial^4 w}{\partial x^4} + \left(\frac{D\Delta_n \Gamma}{p^* L^2}\right) \widehat{T} \frac{\partial^2 w}{\partial x^2} + \left(w - \frac{W_0}{\Delta_n}\right) \exp\left[1 - \left(w - \frac{W_0}{\Delta_n}\right)\right] - \left(\frac{\mu \mathscr{Q} L^2}{\Delta_n^3 p^*}\right) p^{\text{fluid}} = 0, \tag{13}$$

where

$$\widehat{T} = 1 - \left(\frac{\Delta_n^2}{L^2 \Gamma}\right) \frac{1}{2(x_R - x_L)} \int_{x_L}^{x_R} \left(\frac{\partial w}{\partial x}\right)^2 \mathrm{d}x, \tag{14}$$

and

$$\frac{\partial w}{\partial t} = 1 - \frac{\partial}{\partial x}\left[\frac{1}{\alpha^2}\left(\frac{2}{\alpha}\tanh\left(\frac{\alpha w}{2}\right) - w\right) \frac{\partial p^{\text{fluid}}}{\partial x}\right], \tag{15}$$

where

$$\alpha = \left(\frac{6\sqrt{5} W_{\min}}{d}\right) \frac{1}{w} \left[1 - \left(\frac{W_{\min}}{\Delta_n}\right) \frac{1}{w}\right]^{-3/2}. \tag{16}$$

Note that we have also neglected the influence of $u$ in the term due to the bond traction. The quantity $\widehat{T}$ represents a dimensionless *compression* in the beam (*i.e.* positive for compression, negative for tension).

## 2.2 Parameter estimation

The simplified one-dimensional model (13)–(16) requires 11 of the 13 constants in Table 1. However, experimental evaluation of many of these parameters is notably deficient.

The least-well characterised parameters are the bond constants. For the maximum normal traction we use the investigation of Gallant *et al.* [7], who deduced the traction forces between a rolling cell and its substrate.

They calculated the tensile part of this stress to be 200 nN. Half the traction at the base of the rolling cell is in tension, and half is in compression, so we estimate the total force to detach the cell to be twice the tensile force, or 400 nN. Finally $p^*$ is the total detaching force per unit area. If the attached area of a cell is estimated to be $(10\,\mu\mathrm{m})^2$, then we find $p^* \approx 4000\,\mathrm{Pa}$. Other bond-related numbers are little more than educated guesses. Given a value of 50 nm for the typical thickness $\Delta_n$ of the fluid layer,[1] we estimate $d$ and $W_0$ to be both around 5 nm, and $W_{\min}$ to be half of this (it must be less than $W_0$).

The fluid viscosity $\mu$ is well-known; we use $\mu \approx 10^{-3}\,\mathrm{Pa\,s}$ [1]. For the pumping rate $\mathscr{Q}$, we appeal to the investigation of Misfeldt *et al.* [11], who found the value of $\mathscr{Q} = 7.3\,\mu\mathrm{l\,cm^{-2}\,hr^{-1}}$, corresponding to an approximate value of $2 \times 10^{-8}\,\mathrm{m\,s^{-1}}$.

For the elastic constants, if we assume that $D$ and $B$ are given by (49) we need representative values for the epithelial shear modulus $G$, Poisson ratio $\nu$, and thickness $h$. Assumption of an incompressible layer gives $\nu = 1/2$. Rothen-Rutishauser *et al.* [14] show a thickness of 6–8 $\mu$m for confluent MDCK cells, so we choose 7 $\mu$m. However, the shear modulus of cells is not well quantified. Lim *et al.* [10] cite a range for $G$ of 10–500 Pa, while Naire and Jensen [12] cite a Young's modulus of 685 Pa. For incompressible materials, this is equal to $3G$. With these investigations in mind we choose $G = 250\,\mathrm{Pa}$ as representative. These give $D \approx 7 \times 10^{-3}\,\mathrm{N\,m^{-1}}$ and $B \approx 1.9 \times 10^{-14}\,\mathrm{N\,m}$. Little is known about the growth strain $\Gamma$, but we will choose $\Gamma = 0.1$. Finally we will assume that the typical dome length is around ten times the cell layer thickness, or $L = 10^{-4}\,\mathrm{m}$.

These values are shown in Table 2 for convenience. We can use these to calculate the dimensionless

| **Quantity** | **Value** |
|---|---|
| $p^*$ | $4000\,\mathrm{Pa}$ |
| $\Delta_n$ | $50\,\mathrm{nm}$ |
| $W_0$ | $5\,\mathrm{nm}$ |
| $W_{\min}$ | $2.5\,\mathrm{nm}$ |
| $d$ | $5\,\mathrm{nm}$ |
| $\mu$ | $10^{-3}\,\mathrm{Pa\,s}$ |
| $\mathscr{Q}$ | $2 \times 10^{-8}\,\mathrm{m\,s^{-1}}$ |
| $B$ | $1.9 \times 10^{-14}\,\mathrm{N\,m}$ |
| $D$ | $7 \times 10^{-3}\,\mathrm{N\,m^{-1}}$ |
| $\Gamma$ | $0.1$ |
| $L$ | $10^{-4}\,\mathrm{m}$ |

Table 2: Typical values for each of the constants appearing in the simplified model.

parameters appearing in (13)–(16), which we will henceforth denote by script capitals:

$$\mathscr{A} := \frac{B\Delta_n}{p^* L^4} = 2.38 \times 10^{-9}, \qquad \mathscr{B} := \frac{D\Delta_n \Gamma}{p^* L^2} = 8.75 \times 10^{-7}, \qquad \mathscr{C} := \frac{W_0}{\Delta_n} = 0.1, \tag{17}$$

$$\mathscr{D} := \frac{\mu \mathscr{Q} L^2}{\Delta_n^3 p^*} = 0.4, \qquad \mathscr{E} := \frac{\Delta_n^2}{L^2 \Gamma} = 2.5 \times 10^{-6}, \qquad \mathscr{F} := \frac{6\sqrt{5} W_{\min}}{d} = 6.71, \tag{18}$$

$$\mathscr{G} := \frac{W_{\min}}{\Delta_n} = 0.05. \tag{19}$$

# 3 Numerical results

In this section we will analyse the one-dimensional system (13)–(16) in order to gain some insights into the doming process. It is straightforward to show that the system admits the uniform solution

$$w = t + \mathscr{C}, \qquad \widehat{T} = 1, \qquad p^{\mathrm{fluid}} = \frac{t\mathrm{e}^{1-t}}{\mathscr{D}}, \tag{20}$$

assuming an initial displacement condition of $w|_{t=0} = \mathscr{C}$. If the model is to predict dome formation, this simple solution must at some point lose its stability, to be replaced by a spatially-varying displacement. The

[1] Paul Appleton, personal communication.

initial onset of this instability is investigated in Section 3.1, and subsequently in Section 3.2 we will solve the full system numerically to elucidate the later evolution of the tissue displacement. We anticipate that the wavelength of this displacement will correspond to the distance between the centres of neighbouring domes, as the peaks of the initial sinusoidal deformation evolve into the characteristic domes seen in *in vitro* experiments.

### 3.1 Linear stability analysis

In order to investigate the onset of instability in the uniform solution (20), we add to that solution small perturbations, *viz.*

$$w = (t + \mathscr{C}) + w_1, \qquad p^{\text{fluid}} = \frac{t\mathrm{e}^{1-t}}{\mathscr{D}} + p_1^{\text{fluid}}, \qquad \widehat{T} = 1 + \widehat{T}_1. \tag{21}$$

This ansatz is substituted into the system (13)–(16), and only linear terms are kept. We obtain

$$\mathscr{A}\frac{\partial^4 w_1}{\partial x^4} + \mathscr{B}\frac{\partial^2 w_1}{\partial x^2} + (1-t)\mathrm{e}^{1-t}w_1 - \mathscr{D}p_1^{\text{fluid}} = 0, \tag{22}$$

$$\widehat{T}_1 = 0, \qquad \frac{\partial w_1}{\partial t} = -F(t)\frac{\partial^2 p_1^{\text{fluid}}}{\partial x^2}, \tag{23}$$

where

$$F(t) = \frac{1}{\alpha_0^2}\left[\frac{2}{\alpha_0}\tanh\left(\frac{\alpha_0(t+\mathscr{C})}{2}\right) - (t+\mathscr{C})\right] \tag{24}$$

and

$$\alpha_0 = \frac{\mathscr{F}}{t+\mathscr{C}}\left[1 - \frac{\mathscr{G}}{t+\mathscr{C}}\right]^{-3/2}. \tag{25}$$

Eliminating $p_1^{\text{fluid}}$ between (22) and $(23)_2$, and searching for sinusoidally-varying profiles of the normal displacement $w = W(t)\mathrm{e}^{i\sigma x}$, we obtain

$$W'(t) = R(t;\sigma)W(t), \tag{26}$$

where

$$R(t;\sigma) = \frac{\sigma^2}{\mathscr{D}}F(t)\left(\mathscr{A}\sigma^4 - \mathscr{B}\sigma^2 + (1-t)\mathrm{e}^{1-t}\right). \tag{27}$$

Thus while $R(t;\sigma) < 0$ the sinusoidal mode with wavenumber $\sigma$ is stable. However as $t$ increases, $R(t;\sigma)$ will become positive. Analysis of (27) indicates that the smallest $t$ for which $R(t;\sigma) = 0$ is given by the solution to $4(1-t)\mathrm{e}^{1-t} = \mathscr{B}^2/\mathscr{A}$, when $\sigma = \sqrt{\mathscr{B}/2\mathscr{A}}$. On using the values in (17), instability first occurs at $t = 0.99992$, and the wavelength of this first instability is $2\pi/\sigma = 0.463$.

Note that $t \approx 1$ is, in dimensional terms, very short (around 2.5 s). We suspect that this is due to a pumping rate which is far too large; perhaps $\mathscr{Q}$ is strongly pressure-dependent, or the results in [11] were inapplicable to our system.

Additionally, the significance of the instability result above is reduced by the realisation that by $t = 1$ all wavelengths in the range $(0.328, \infty)$ have become unstable and will grow. Thus, in order to evaluate the key wavelength of deformation (which will indicate the dome peak-to-peak distance) we must go beyond this elementary analysis to calculate the full numerical solution. This should allow us to identify the mode which grows fastest, or to note the coalescence of smaller waves, either of which will hopefully give a representative wavelength which compares well with *in vitro* experiments.

### 3.2 Full numerical solution of the system

We approximate solutions to the reduced one-dimensional model using a simple method-of-lines approach with centred differences for spatial derivatives. This is similar approach to a method suggested in Flitton and King [6] for a related sixth-order parabolic system.

For numerical purposes, we write the model in the equivalent form

$$\frac{\partial w}{\partial t} = 1 - \frac{\partial q}{\partial x} \tag{28}$$

$$q = -\frac{\kappa}{\alpha^2}\frac{\partial p}{\partial x} \tag{29}$$

$$p = \frac{1}{D}\left\{(w-C)\exp\left(1-(w-C)\right) - A\frac{\partial^2 m}{\partial x^2} - B\widehat{T}m\right\} \tag{30}$$

$$m = -\frac{\partial^2 w}{\partial x^2} \tag{31}$$

$$\widehat{T} = 1 - \frac{E}{2X}\int_0^X \left(\frac{\partial w}{\partial x}\right)^2 \mathrm{d}x \tag{32}$$

$$\alpha = \frac{F}{w}\left(1-\frac{G}{w}\right)^{-3/2} \tag{33}$$

$$\kappa = w - \frac{2}{\alpha}\tanh\left(\frac{\alpha w}{2}\right) \tag{34}$$

introducing the new variables $q$, the flux of fluid, and $m$, the curvature of the cell layer (here taking $\kappa$ to be positive). We discretize the domain $0 < x < X$ into $N$ regions of length $h = X/N$, and approximate the dependent variables $w$, $p$ and $x$ by their values $w_1, w_2, \ldots, w_N$ *etc.* at the mid-points of the regions ($x = (n-\frac{1}{2})h$); however, the flux $q$ is approximated by its values $q_0, q_1, \ldots, q_N$ at the end-points of the regions ($x = nh$). All derivatives are replaced by central differences; the integral in (32) is approximated by the trapezium rule using the values of the integrand at the ends of the regions. The resulting semi-discrete system of equations is

$$\frac{dw_n}{dt} = 1 - \frac{q_n - q_{n-1}}{h} \tag{35}$$

$$q_n = -\frac{\kappa_n}{\alpha_n^2}\frac{p_{n+1}-p_n}{h} \tag{36}$$

$$p_n = \frac{1}{D}\left\{(w_n-C)\exp\left(1-(w_n-C)\right) - A\left(\frac{m_{n-1}-2m_n+m_{n+1}}{h^2}\right) - B\widehat{T}m_n\right\} \tag{37}$$

$$m_n = -\frac{w_{n-1}-2w_n+w_{n+1}}{h^2} \tag{38}$$

$$\widehat{T} = 1 - \frac{Eh}{2X}\left\{\frac{1}{2}\left(\frac{w_1-w_0}{h}\right)^2 + \sum_{j=1}^{N-1}\left(\frac{w_{j+1}-w_j}{h}\right)^2 + \frac{1}{2}\left(\frac{w_{N+1}-w_N}{h}\right)^2\right\} \tag{39}$$

$$\alpha_n = \frac{2F}{w_{n+1}+w_n}\left(1-\frac{2G}{w_{n+1}+w_n}\right)^{-3/2} \tag{40}$$

$$\kappa_n = \frac{w_{n+1}+w_n}{2} - \frac{2}{\alpha_n}\tanh\left(\frac{\alpha_n(w_{n+1}+w_n)}{4}\right) \tag{41}$$

where (35), (37) and (38) hold for $n = 1, \ldots, N$, and (36), (40) and (41) hold for $n = 0, \ldots, N$. The values of $w_0$, $w_{N+1}$, $m_0$ and $m_{N+1}$ are specified by the boundary conditions, which are chosen to be that the first derivatives of $w$ and $m$, along with the flux $q$, are zero at both ends of the domain ($x = 0, X$). For our discretized equations, these correspond to $w_0 = w_1$, $w_{N+1} = w_N$, $m_0 = m_1$, $m_{N+1} = m_N$, $q_0 = q_N = 0$. The resulting system of ordinary differential equations for $w_n$ are solved using the MATLAB routine `ode15s` (an implicit solver; the Jacobian is calculated using numerical differencing, exploiting its banded structure for efficiency).

The initial conditions are taken to be $w_n = w_{uni}$, but in order to initiate the instability in a controlled manner we perturb the uniform solution slightly at one point, setting $w_{N/2} = w_{uni} + \epsilon$. Other options considered include the addition of random noise at all points, or the forcing of the system with a predetermined mode. The former of these in particular seems to be ill-advised, due to the in-built error-control of the ODE solver. We take $w_{uni} = 1.0$, so that the system is initially linearly stable, but we expect instabilities to develop when $t \simeq 0.1$. We take the length of the domain to be $X = 20$.[2]

We first examine the behaviour of numerical solutions with the original parameter values. With $\epsilon = 0$, the instability does not develop. Setting $\epsilon = 1.0 \times 10^{-6}$, we obtain the plots in Figure 2. While the aspect ratio of these plots is distorted (with the vertical variations being greatly exaggerated), the length-scale of the resulting solutions is clearly far less than that observed in experiments. This could indicate an flaw in the numerical scheme used here; however, it is not inconsistent with the linear stability analysis. From the linear instability analysis, the first mode to become unstable have wavelength 0.463, which is shorter than the desired dome size. Furthermore, shortly after the time at which this mode becomes unstable, shorter-wavelength modes are not only unstable but grow substantially faster than the first mode. This is a consequence of the $\sigma^2$ term at the start of (27). These shorter wavelength modes then outcompete the first mode and develop into domes with even smaller wavelengths. There doesn't appear to be any competition or merging between domes; this may happen too slowly, or it may be that the nonlinearity in the cell–substrate bonding force isn't of the right form.[3]

The unavoidable conclusion that we draw from this is that the pumping rate used earlier is probably not appropriate for the current model; the layer is not leaky, so the mean height of the layer must increase to accommodate it. As noted above $t \simeq 1$ corresponds to 2.5 s in dimensionless terms; decreasing the pumping rate by two or three orders of magnitude seems to be called for. As such, we now take $D$ to be 0.01 of its original value (which only changes $D$). The first mode to become unstable has $\sigma = \sqrt{B/2A} = \sqrt{12\Gamma}L/h$; as the estimate for $h$ is roughly correct, and the material parameters don't enter into the estimate, this suggests that we should reduce the layer strain $\Gamma$ substantially, so we take $\Gamma = 0.01$. However, even these changes do not appear to tame the short-wavelength modes, as can be seen in Figure 4. Further changes need to be made in order to inhibit the growth of short-wavelength modes, perhaps by greatly increasing the bending stiffness of the layer.

# 4 Conclusion and further research

The results of the precious section, while rather disappointing overall as a prediction of doming behaviour, at least indicated that the proposed mechanism of dome formation displayed in Figure 1 gave rise to an undulating epithelium, which we regard as the precursor of doming. The main disappointment is in the final wavelength of the undulations; the numerical values of the parameters derived in Section 2.2 gave a wavelength which was absurdly short (see Figure 2). By varying these parameters, the characteristic wavelength may be altered, and as such we may be able to obtain physically-realistic doming patterns. However, the changes in the physical parameters must also be justified for this approach to have any merit.

If the model can be furnished with these more realistic parameters, we may consider additions and enhancements to the model. We could consider using the full two-dimensional formulation of the equations in order to examine how domes may be spatially arranged. Furthermore we could consider the breakage and reformation of domes; if the stress in a dome becomes too large we could artificially let it 'deflate'; however, the bonds will not reform due to this process, so an equation for the maximum bond strength $p^*$ must be furnished to reflect this. In the study group the equation mooted was of the form

$$\frac{\mathrm{d}p^*}{\mathrm{d}t} = -\beta(w - W_0)_+ p^*. \tag{42}$$

One could also give an equation for the growth strain $\gamma_{\alpha\beta}$ which reflected the slowing of growth as the layer reached confluence; however, this is a very complex problem that is still quite poorly understood.

[2] While a longer domain would be ideal, memory constraints within MATLAB limit $N \lesssim 4000$, and as such the dominant short-wavelength mode would not be resolved by a larger domain.

[3] One might speculate that these oscillations are caused by the numerical method — particularly as the conservation of mass equation is not upwinded — but simulations on the smaller domain $X = 1$, with $N = 100, 400, 1000, 4000$, all give domes with wavelength about 0.09, which suggests that the numerical method is reasonably accurate.

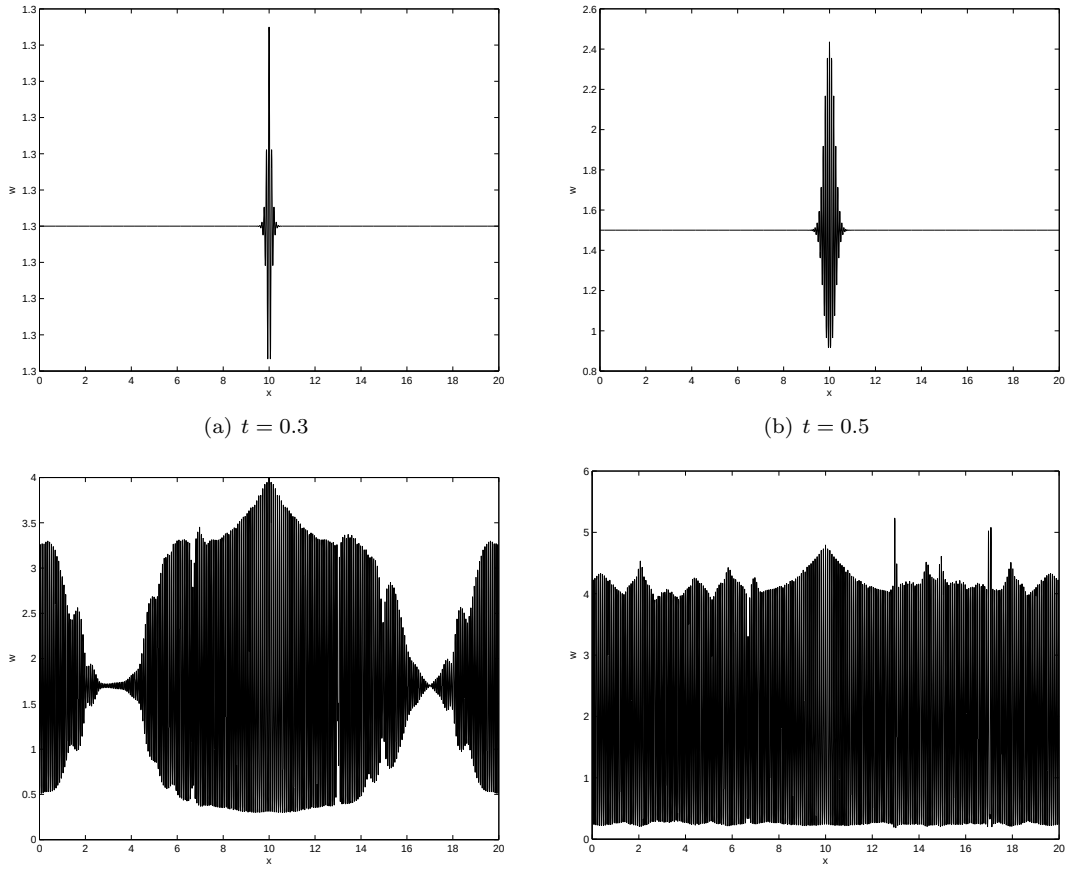


(a) $t = 0.3$ (b) $t = 0.5$

(c) $t = 0.7$ (d) $t = 1.0$

Figure 2: Numerical simulations with original parameter values; here $X = 20$, $N = 4000$, and the uniform initial state $w_n = 1$ is perturbed by setting $w_{2000} = 1 + 10^{-6}$.

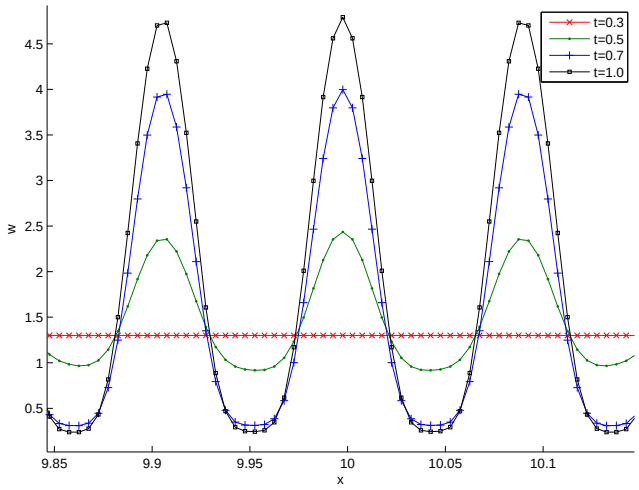


Figure 3: Behaviour near $X = 10$ for the simulations in Figure 2, illustrating that the small length-scale oscillations are resolved by the discrete grid.

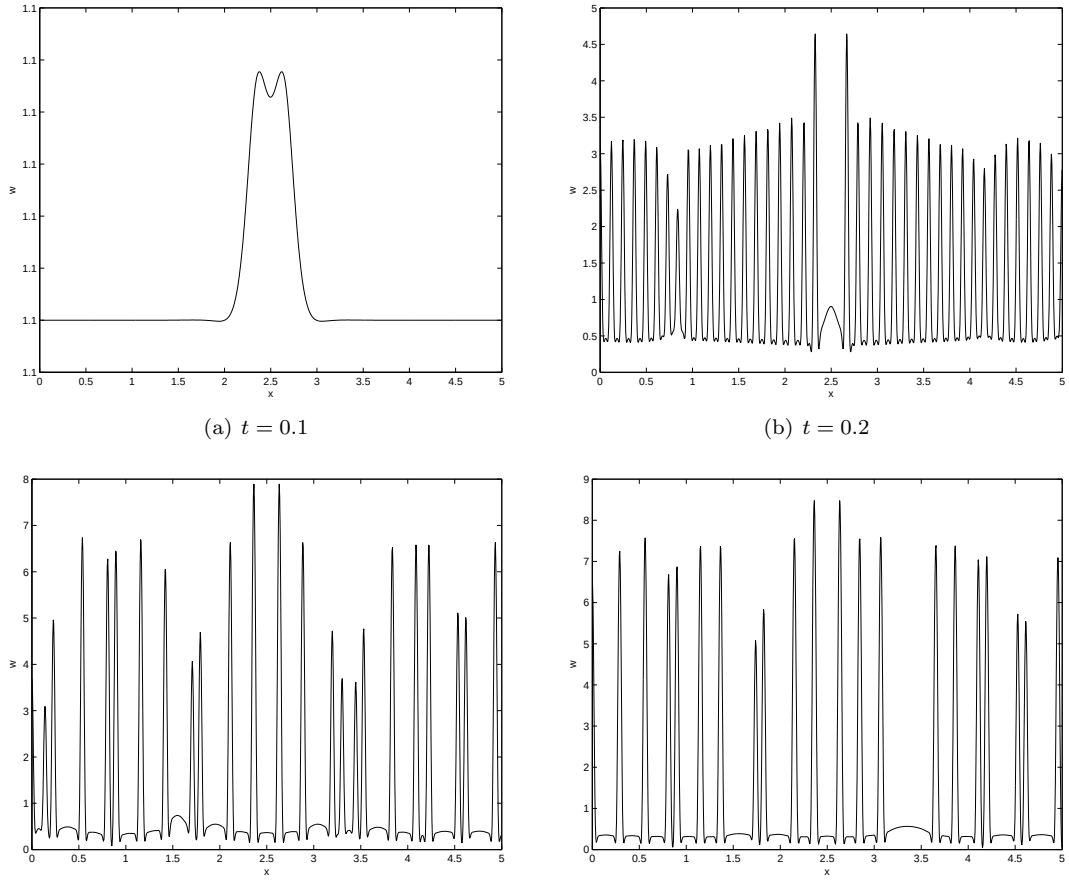


(a) $t = 0.1$ (b) $t = 0.2$

(c) $t = 0.3$ (d) $t = 0.4$

Figure 4: Numerical simulations with modified parameter values (reduced pumping rate and layer strain). Note that the integration breaks down for some reason when $t \simeq 0.52$.

Finally one could consider extending the model to include more realistic expressions for the bond strength and epithelial layer mechanical properties; it is not clear that such modifications would enhance the accuracy of the model without sacrificing its relative simplicity.

# A Derivation of the governing equations

We will model the doming process by assuming that the epithelial cell layer itself is a solid plate, and that the bonding between the cell layer and the substrate is a porous adhesive layer.

We begin by considering the solid plate. As noted, this plate will be stressed due to the growth of the cells. Such a growing plate was considered by Dervaux *et al.* [4]. We will use this model in the subsequent analysis.

Let $w$ be the normal displacement of the middle-surface of the plate, which has thickness $h$, shear modulus $G$ and Poisson ratio $\nu$. If the in-plane displacement field is $u_\alpha$, then the middle-surface strain tensor $\gamma_{\alpha\beta}$ and the change-of-curvature tensor $\rho_{\alpha\beta}$ are

$$\gamma_{\alpha\beta} = \frac{1}{2}(u_{\alpha,\beta} + u_{\beta,\alpha}) + \frac{1}{2}w_{,\alpha}w_{,\beta}, \tag{43}$$

$$\rho_{\alpha\beta} = w_{,\alpha\beta}, \tag{44}$$

where a subscript preceded by a comma indicates partial differentiation. The equations of equilibrium in

terms of the stress resultant tensor $n_{\alpha\beta}$ and the moment resultant tensor $m_{\alpha\beta}$ are

$$n_{\beta\alpha,\beta} + p_\alpha = 0, \tag{45}$$

$$m_{\alpha\beta,\alpha\beta} - w_{,\alpha\beta} n_{\alpha\beta} - p_3 = 0, \tag{46}$$

where $p_3$ is the normal surface traction and $p_\alpha$ are the tangential surface tractions.

To close the system we need constitutive relations between $n_{\alpha\beta}$ and $\gamma_{\alpha\beta}$, and between $m_{\alpha\beta}$ and $\rho_{\alpha\beta}$. These are given by the linear relations

$$n_{\alpha\beta} = DA_{\alpha\beta\lambda\mu}(\gamma_{\lambda\mu} - \gamma^{\mathrm{g}}_{\lambda\mu}), \tag{47}$$

$$m_{\alpha\beta} = BA_{\alpha\beta\lambda\mu}\rho_{\lambda\mu}, \tag{48}$$

where

$$D = \frac{2Gh}{1-\nu}, \qquad B = \frac{Gh^3}{6(1-\nu)}, \tag{49}$$

and

$$A_{\alpha\beta\lambda\mu} = \left(\frac{1-\nu}{2}\right)(\delta_{\alpha\lambda}\delta_{\beta\mu} + \delta_{\alpha\mu}\delta_{\beta\lambda}) + \nu\delta_{\alpha\beta}\delta_{\lambda\mu}, \tag{50}$$

where $\delta_{\alpha\beta}$ is Kronecker's delta.

Now, the solution to (45) can be written in terms of an Airy stress function $\chi$:

$$n_{\alpha\beta} = P_{\alpha\beta} + \varepsilon_{\alpha\lambda}\varepsilon_{\beta\mu}\chi_{,\lambda\mu}, \tag{51}$$

where $P_{\alpha\beta}$ is a particular solution of (45) and $\varepsilon_{\alpha\beta}$ is the two-dimensional Levi-Civita symbol ($\varepsilon_{11} = \varepsilon_{22} = 0$, $\varepsilon_{12} = 1$, $\varepsilon_{21} = -1$). On inverting (47) we find that

$$\gamma_{\alpha\beta} = \gamma^{\mathrm{g}}_{\alpha\beta} + \frac{1}{D}E_{\alpha\beta\lambda\mu}n_{\lambda\mu}, \tag{52}$$

where

$$E_{\alpha\beta\lambda\mu} = \frac{1}{2(1-\nu)}(\delta_{\alpha\lambda}\delta_{\beta\mu} + \delta_{\alpha\mu}\delta_{\beta\lambda}) - \frac{\nu}{(1-\nu^2)}\delta_{\alpha\beta}\delta_{\lambda\mu}. \tag{53}$$

Combining (51) and (52) gives us

$$\gamma_{\alpha\beta} = \Gamma_{\alpha\beta} + \frac{1}{D}\varepsilon_{\lambda\gamma}\varepsilon_{\mu\delta}E_{\alpha\beta\lambda\mu}\chi_{,\gamma\delta} \tag{54}$$

where

$$\Gamma_{\alpha\beta} = \gamma^{\mathrm{g}}_{\alpha\beta} + \frac{1}{D}E_{\alpha\beta\lambda\mu}P_{\lambda\mu}. \tag{55}$$

Now we substitute (44) and (51) into (48) and (46) to obtain

$$B\nabla^4 w - P_{\alpha\beta}w_{,\alpha\beta} - 2[w,\chi] - p_3 = 0, \tag{56}$$

where

$$[A,B] = \frac{1}{2}\varepsilon_{\alpha\lambda}\varepsilon_{\beta\mu}A_{,\alpha\beta}B_{,\lambda\mu} = \frac{1}{2}\left(A_{,11}A_{,22} + A_{,22}B_{,11} - 2A_{,12}B_{,12}\right). \tag{57}$$

Secondly we substitute $\gamma_{\alpha\beta}$ from (54) into the compatibility condition [8]

$$\varepsilon_{\alpha\beta}\varepsilon_{\lambda\mu}\left(\gamma_{\alpha\mu,\beta\lambda} + \frac{1}{2}w_{,\alpha\mu}w_{,\beta\lambda}\right) = 0. \tag{58}$$

This becomes

$$\frac{1}{D(1-\nu^2)}\nabla^4\chi + [w,w] = \varepsilon_{\alpha\beta}\varepsilon_{\lambda\mu}\Gamma_{\alpha\mu,\beta\lambda}. \tag{59}$$

For convenience we write down the full system of equations for the elastic plate, from (43), (54), (56) and (59):

$$\frac{1}{2}(u_{\alpha,\beta}+u_{\beta,\alpha}) + \frac{1}{2}w_{,\alpha}w_{,\beta} = \gamma^{\mathrm{g}}_{\alpha\beta} + \frac{1}{D}E_{\alpha\beta\lambda\mu}P_{\lambda\mu} + \frac{1}{D}\varepsilon_{\lambda\gamma}\varepsilon_{\mu\delta}E_{\alpha\beta\lambda\mu}\chi_{,\gamma\delta}, \tag{60}$$

$$P_{\alpha\beta,\beta} + p_\alpha = 0 \qquad \text{(particular solution)}, \tag{61}$$

$$B\nabla^4 w - P_{\alpha\beta}w_{,\alpha\beta} - 2[w,\chi] - p_3 = 0, \tag{62}$$

$$\frac{1}{D(1-\nu^2)}\nabla^4\chi + [w,w] = \varepsilon_{\alpha\beta}\varepsilon_{\lambda\mu}\left(\gamma^{\mathrm{g}}_{\alpha\mu,\beta\lambda} + \frac{1}{D}E_{\alpha\mu\gamma\delta}P_{\gamma\delta,\beta\lambda}\right). \tag{63}$$

Equations (62) and (63) are the Föppl–von Karman equations which govern the deformation of the plate, and are to be solved for $w$ and $\chi$.

Next we consider the bonding layer between the tissue and the substrate. This will enter the model through a number of equations which will couple the plate displacements $u_\alpha$ and $w$ with the traction terms $p_\alpha$ and $p_3$. The traction terms will have two components, namely those due to the fluid pressure and those due to the protein bonds between the cells and the substrate. Neglecting the tangential traction due to the fluid, we have

$$p_\alpha = p^{\mathrm{bond}}_\alpha \qquad \text{and} \qquad p_3 = p^{\mathrm{fluid}} + p^{\mathrm{bond}}_3. \tag{64}$$

Considering the bonds first of all, we use the model of Needleman [13]. His analysis was for a one-dimensional surface delaminating from a substrate, but it is easily extended to a two-dimensional plate. Identifying the displacement of the bottom surface of the plate with that of the centre-surface (*i.e.* $u_1$, $u_2$, $w$) we have a decohesion potential $\phi$, from which the tractions in the $x$, $y$ and $z$-directions can be retrieved:

$$p^{\mathrm{bond}}_1 = -\frac{\partial\phi}{\partial u_1}, \qquad p^{\mathrm{bond}}_2 = -\frac{\partial\phi}{\partial u_2}, \qquad p^{\mathrm{bond}}_3 = -\frac{\partial\phi}{\partial w}. \tag{65}$$

The suggested form for $\phi$ is

$$\phi = p^*\mathrm{e}^1\Delta_n\left\{1 - \left(1 + \frac{(w-W_0)}{\Delta_n}\right)\exp\left(-\frac{(u_1^2+u_2^2)}{\Delta_t^2} - \frac{(w-W_0)}{\Delta_n}\right)\right\} \tag{66}$$

so that

$$(p^{\mathrm{bond}}_1, p^{\mathrm{bond}}_2) = -p^*\left(1 + \frac{(w-W_0)}{\Delta_n}\right)\exp\left(1 - \frac{(u_1^2+u_2^2)}{\Delta_t^2} - \frac{(w-W_0)}{\Delta_n}\right)\frac{2\Delta_n}{\Delta_t^2}(u_1,u_2), \tag{67}$$

$$p^{\mathrm{bond}}_3 = -p^*\left(\frac{(w-W_0)}{\Delta_n}\right)\exp\left(1 - \frac{(u_1^2+u_2^2)}{\Delta_t^2} - \frac{(w-W_0)}{\Delta_n}\right). \tag{68}$$

In these expressions, $W_0$ is the 'natural' length of the bonds, so that if $w < W_0$, the normal traction is repulsive. In Needleman's original model, $W_0$ was zero. A sketch of $p^{\mathrm{bond}}_3$ with $u_1 = u_2 = 0$ can be seen in Figure 5.

Finally we need to consider the fluid flow through the bonding layer. We use the Brinkman equation,

$$\mu\left(\widehat{\nabla}^2\boldsymbol{v} - \frac{1}{K}\boldsymbol{v}\right) = \widehat{\boldsymbol{\nabla}}p^{\mathrm{fluid}} \qquad \text{with} \qquad \widehat{\boldsymbol{\nabla}}\cdot\boldsymbol{v} = 0, \tag{69}$$

where $\boldsymbol{v}$ is the three-dimensional velocity, $\mu$ is the viscosity, $p^{\mathrm{fluid}}$ is the hydrostatic pressure, and $K$ is the permeability of the layer, which is dependent on the fluid layer thickness $w$. The notation $\widehat{\boldsymbol{\nabla}}$ indicates that the gradient operator is defined over three dimensions rather than two (*cf.* (56) and (59) ).

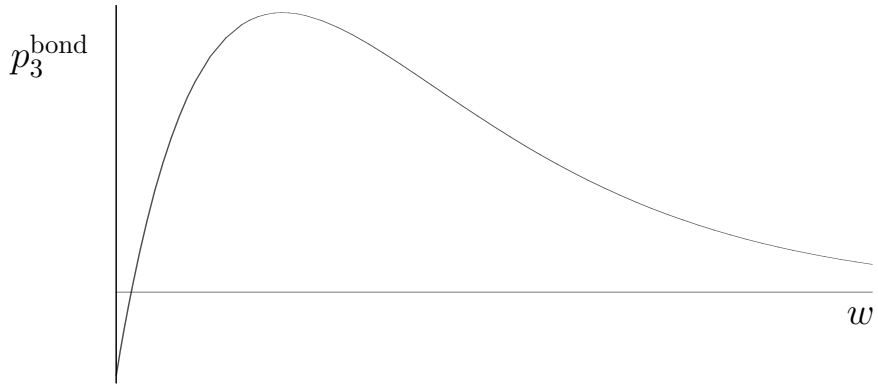


Figure 5: A sketch of the form of Needleman's bond function $p_3^{\text{bond}}$ with $u_1 = u_2 = 0$.

The boundary conditions for the fluid are

$$v_1 = v_2 = v_3 = 0 \qquad \text{at} \qquad z = 0 \qquad \text{(the substrate)}, \tag{70}$$

$$v_1 = v_2 = 0 \qquad \text{and} \qquad v_3 = \frac{\partial w}{\partial t} - Q \qquad \text{at} \qquad z = w \qquad \text{(the plate–fluid interface)}, \tag{71}$$

where $Q$ is the rate of fluid volume increase per unit area, due to the pumping action of the cell layer. The traction conditions will be given by (64).

We also need to find a plausible expression for $K[w]$, the permeability of the layer in terms of its thickness. Not many analytical expressions exist. Feng and Weinbaum [5] developed a semi-numerical relation, in the context of flow through the fibres emerging from the surface of a red blood cell. However, this is still an approximation and the exact form shouldn't qualitatively change the overall system behaviour. One of the most common *analytic* expressions used in the literature (even though it ostensibly applies only to granular materials) is the Kozeny–Carman law [3]. In this relation if $d$ is the mean particle size, and $n$ is the porosity, then

$$K = \frac{d^2}{180} \frac{n^3}{(1-n)^2}. \tag{72}$$

Obviously our layer is not composed of a granular medium, and as such we identify $d$ with the typical distance between the bonds that form the layer. Now the question we need to ask is how the porosity $n$ depends on the fluid layer thickness $w$. We will assume that the amount of 'solid phase' (*i.e.* bond material) remains unchanged under stretching, and so $n = (w - W_{\min})/w$, where $W_{\min}$ is the theoretical displacement of the layer at which its fluid content is zero. Thus

$$K = \frac{d^2}{180 W_{\min}^2} w^2 \left(1 - \frac{W_{\min}}{w}\right)^3. \tag{73}$$

## A.1 Nondimensionalisation

We will choose the following scalings, where a tilde denotes a dimensionless quantity:

$$(x, y, z) = (L\widetilde{x}, L\widetilde{y}, \Delta_n \widetilde{z}), \tag{74}$$

$$(u_1, u_2, w) = (\Delta_t \widetilde{u}_1, \Delta_t \widetilde{u}_2, \Delta_n \widetilde{w}), \tag{75}$$

$$(v_1, v_2, v_3) = (\mathscr{V}\widetilde{v}_1, \mathscr{V}\widetilde{v}_2, \varepsilon\mathscr{V}\widetilde{v}_3), \tag{76}$$

$$p^{\text{fluid}} = \frac{\mu \mathscr{V} L}{\Delta_n^2} \widetilde{p}^{\text{fluid}}, \tag{77}$$

$$p_\alpha = p^* \widetilde{p}_\alpha, \qquad p_3 = p^* \widetilde{p}_3, \qquad \gamma^{\text{g}}_{\alpha\beta} = \Gamma \widetilde{\gamma}^{\text{g}}_{\alpha\beta}, \tag{78}$$

$$t = \frac{L}{\mathscr{V}} \widetilde{t}, \qquad Q = \mathscr{Q}\widetilde{Q}. \tag{79}$$

In these expressions $L$ is the typical lateral lengthscale of a dome, $\mathscr{V}$ is the (undetermined) typical lateral velocity scale, and $\varepsilon$ is the aspect ratio,

$$\varepsilon = \frac{\Delta_n}{L}. \tag{80}$$

The scaling for the fluid hydrostatic pressure is typical for Stokes flow, and applying the scalings above to $(69)_1$ gives (dropping the tilde notation)

$$\frac{\partial p^{\text{fluid}}}{\partial x} = \varepsilon^2 \nabla^2 v_1 + \frac{\partial^2 v_1}{\partial z^2} - \alpha^2 v_1, \tag{81}$$

$$\frac{\partial p^{\text{fluid}}}{\partial y} = \varepsilon^2 \nabla^2 v_2 + \frac{\partial^2 v_2}{\partial z^2} - \alpha^2 v_2, \tag{82}$$

$$\frac{\partial p^{\text{fluid}}}{\partial z} = \varepsilon^4 \nabla^2 v_3 + \varepsilon^2 \frac{\partial^2 v_3}{\partial z^2} - \varepsilon^2 \alpha^2 v_3, \tag{83}$$

$$\frac{\partial v_1}{\partial x} + \frac{\partial v_2}{\partial y} + \frac{\partial v_3}{\partial z} = 0, \tag{84}$$

where $\alpha = \Delta_n / \sqrt{K}$ is a function of fluid thickness $w$, given by

$$\alpha = \frac{6\sqrt{5} W_{\min}}{d} \frac{1}{w} \left(1 - \frac{W_{\min}}{\Delta_n w}\right)^{-3/2}. \tag{85}$$

Assuming $\varepsilon \ll 1$ and omitting terms of $O(\varepsilon^2)$, we obtain

$$\frac{\partial p^{\text{fluid}}}{\partial x} = \frac{\partial^2 v_1}{\partial z^2} - \alpha^2 v_1, \tag{86}$$

$$\frac{\partial p^{\text{fluid}}}{\partial y} = \frac{\partial^2 v_2}{\partial z^2} - \alpha^2 v_2, \tag{87}$$

$$\frac{\partial p^{\text{fluid}}}{\partial z} = 0, \tag{88}$$

so that $p^{\text{fluid}} = p^{\text{fluid}}(x, y)$ and

$$v_1 = A(x, y) \cosh \alpha z + B(x, y) \sinh \alpha z - \frac{1}{\alpha^2} \frac{\partial p^{\text{fluid}}}{\partial x}, \tag{89}$$

$$v_2 = C(x, y) \cosh \alpha z + D(x, y) \sinh \alpha z - \frac{1}{\alpha^2} \frac{\partial p^{\text{fluid}}}{\partial y}, \tag{90}$$

for arbitrary functions $A$, $B$, $C$, and $D$. Applying the no-tangential-slip condition at $z = 0$ and $z = w(x, y)$, we eventually obtain

$$v_\kappa = \left\{ (1 - \cosh \alpha w) \frac{\sinh \alpha z}{\sinh \alpha w} + \cosh \alpha z - 1 \right\} \frac{1}{\alpha^2} p^{\text{fluid}}_{,\kappa}. \tag{91}$$

From (84) we have

$$\frac{\partial v_3}{\partial z} = -\boldsymbol{\nabla} \cdot (v_1, v_2), \tag{92}$$

which we integrate over $z \in (0, w(x, y))$, giving

$$v_3|_{z=w(x,y)} - v_3|_{z=0} = -\boldsymbol{\nabla} \cdot \left( \frac{\kappa}{\alpha^2} \boldsymbol{\nabla} p^{\text{fluid}} \right), \tag{93}$$

where

$$\kappa = \kappa[w] = \int_0^{w(x,y)} \left\{ (1 - \cosh \alpha w) \frac{\sinh \alpha z}{\sinh \alpha w} + \cosh \alpha z - 1 \right\} \mathrm{d}z. \tag{94}$$

Now, nondimensionalising the boundary condition (71) at the fluid–plate interface, and defining $\mathscr{V} = \mathscr{Q}/\varepsilon$, we obtain $v_3|_{z=w} = \partial w/\partial t - Q$ (omitting tilde notations again), so that (with no-slip conditions at $z = 0$),

$$\frac{\partial w}{\partial t} = Q - \boldsymbol{\nabla} \cdot \left( \frac{\kappa}{\alpha^2} \boldsymbol{\nabla} p^{\text{fluid}} \right). \tag{95}$$

Further calculations show that

$$\kappa[w] = \frac{2}{\alpha} \tanh \frac{\alpha w}{2} - w. \tag{96}$$

Note that $\kappa$ is negative for all positive values of $w$ and $\alpha$.

The tractions applied to the plate, in their nondimensional form, are given by

$$p_\alpha = -\frac{2\Delta_n}{\Delta_t} \left( 1 + w - \frac{W_0}{\Delta_n} \right) \exp\left( 1 - u_1^2 - u_2^2 - \left( w - \frac{W_0}{\Delta_n} \right) \right) u_\alpha, \tag{97}$$

$$p_3 = -\left( w - \frac{W_0}{\Delta_n} \right) \exp\left( 1 - u_1^2 - u_2^2 - \left( w - \frac{W_0}{\Delta_n} \right) \right) + \left( \frac{\mu \mathscr{Q} L^2}{\Delta_n^3 p^*} \right) p^{\text{fluid}}. \tag{98}$$

Finally, we consider the plate equations. Using the scalings $\chi = DL\Delta_t \widetilde{\chi}$ and $P_{\alpha\beta} = p^* L \widetilde{P}_{\alpha\beta}$, equations (60)–(63) become

$$\frac{1}{2}(u_{\alpha,\beta} + u_{\beta,\alpha}) + \left( \frac{\Delta_n^2}{\Delta_t L} \right) \frac{1}{2} w_{,\alpha} w_{,\beta} = \left( \frac{L\Gamma}{\Delta_t} \right) \gamma^{\text{g}}_{\alpha\beta} + \left( \frac{L^2 p^*}{D\Delta_t} \right) E_{\alpha\beta\lambda\mu} P_{\lambda\mu} + \varepsilon_{\lambda\gamma} \varepsilon_{\mu\delta} E_{\alpha\beta\lambda\mu} \chi_{,\gamma\delta}, \tag{99}$$

$$P_{\alpha\beta,\beta} + p_\alpha = 0 \qquad \text{(particular solution)}, \tag{100}$$

$$\left( \frac{B\Delta_n}{p^* L^4} \right) \nabla^4 w - \varepsilon P_{\alpha\beta} w_{,\alpha\beta} - 2 \left( \frac{D\Delta_n \Delta_t}{p^* L^3} \right) [w, \chi] - p_3 = 0, \tag{101}$$

$$\left( \frac{\Delta_t}{L\Gamma(1-\nu^2)} \right) \nabla^4 \chi + \left( \frac{\Delta_n^2}{\Gamma L^2} \right) [w, w] = \varepsilon_{\alpha\beta} \varepsilon_{\lambda\mu} \left( \gamma^{\text{g}}_{\alpha\mu,\beta\lambda} + \left( \frac{Lp^*}{D\Gamma} \right) E_{\alpha\mu\gamma\delta} P_{\gamma\delta,\beta\lambda} \right). \tag{102}$$

# References


[1] D.J. Acheson. *Elementary Fluid Dynamics*. Oxford University Press, 1990.

[2] N. Auersperg. Histogenetic behavior of tumors. I. Morphologic variation in vitro and in vivo of two related human carcinoma cell lines. *Journal of the National Cancer Institute*, **43**(1):151–173, 1969.

[3] J. Bear. *Dynamics of fluids in porous media*. Dover, New York, 1988.

[4] J. Dervaux, P. Ciarletta, and M. Ben Amar. Morphogenesis of thin hyperelastic plastes: a constitutive theory of biological growth in the Föppl–von Kármán limit. *Journal of the Mechanics and Physics of Solids*, **57**(3):458–471, 2009.
doi:10.1016/j.jmps.2008.11.011

[5] J. Feng and S. Weinbaum. Lubrication theory in highly compressible porous media: the mechanics of skiing, from red cells to humans. *Journal of Fluid Mechanics*, **422**:281–317, 2000.
doi:10.1017/S0022112000001725

[6] J.C. Flitton and J.R. King. Moving-boundary and fixed-domain problems for a sixth-order thin-film equation. *European Journal of Applied Mathematics*, **15**(6):713–754, 2004.
doi:10.1017/S0956792504005753

[7] N.D. Gallant, K.E. Michael, and A.J. García. Cell adhesion strengthening: contributions of adhesive area, integrin binding, and focal adhesion assembly. *Molecular Biology of the Cell*, **16**(9):4329–4340, 2005.
doi:10.1091/mbc.E05-02-0170

[8] W.T. Koiter. On the nonlinear theory of thin elastic shells. *Proceedings of the Koninklijke Nederlandse Akademie van Wetenschappen (Royal Dutch Academy of Sciences), Ser. B*, **69**:1–54, 1966.

[9] J. Leighton, Z. Brada, L.W. Estes, and G. Justh. Secretory activity and oncogenicity of a cell line (MDCK) derived from canine kidney. *Science*, **163**(3866):472–473, 1969.

[10] C.T. Lim, E.H. Zhou, and S.T. Quek. Mechanical models for living cells — a review. *Journal of Biomechanics*, **39**(2):195–216, 2006.
doi:10.1016/j.jbiomech.2004.12.008

[11] D.S. Misfeldt, S.T. Hamamoto, and D.R. Pitelka. Transepithelial transport in cell culture. *Proceedings of the National Academy of Sciences of the United States of America*, **73**(4):1212–1216, 1976.
doi:10.1073/pnas.73.4.1212

[12] S. Naire and O.E. Jensen. Epithelial cell deformation during surfactant-mediated airway reopening: a theoretical model. *Journal of Applied Physiology*, **99**(2):458–471, 2005.
doi:10.1152/japplphysiol.00796.2004

[13] A. Needleman. Micromechanical modelling of interfacial decohesion. *Ultramicroscopy*, **40**(3):203–214, 1992.
doi:10.1016/0304-3991(92)90117-3

[14] B. Rothen-Rutishauser, S.D. Krämer, A. Braun, M. Günthert, and H. Wunderli-Allenspach. MDCK cell cultures as an epithelial in vitro model: cytoskeleton and tight junctions as indicators for the definition of age-related stages by confocal microscopy. *Pharmaceutical Research*, **15**(7):964–971, 1998.
doi:10.1023/A:1011953405272

[15] C. Tanner, D.A. Frambach, and D.S. Misfeldt. Transepithelial transport in cell culture. A theoretical and experimental analysis of the biophysical properties of domes. *Biophysical Journal*, **32**(2):183–190, 1983.
doi:10.1016/S0006-3495(83)84339-2